Magnetic Properties of Quadruple Perovskites $Ba_4LnRu_3O_{12}$ (Ln = La, Nd, Sm-Gd, Dy-Lu)

Yuki Shimoda, Yoshihiro Doi, Makoto Wakeshima and Yukio Hinatsu

Division of Chemistry, Hokkaido University, Sapporo 060-0810, Japan

Abstract

Quadruple perovskites $Ba_4LnRu_3O_{12}$ (Ln = La, Nd, Sm-Gd, Dy-Lu) were prepared and their magnetic properties were investigated. They adopt the 12L-perovskite-type structure consisting of Ru_3O_{12} trimers and LnO_6 octahedra. All of these compounds show an antiferromagnetic transition at 2.5 - 30 K. For $Ba_4NdRu_3O_{12}$, ferrimagnetic ordering has been observed at 11.5 K. The observed magnetic transition is due to the magnetic behavior of the $Ru^{4.33+}{}_3O_{12}$ trimer with $S = 1/2$. Magnetic properties of $Ba_4LnRu_3O_{12}$ were compared with those of triple perovskites $Ba_3LnRu_2O_9$ and double perovskites Ba_2LnRuO_6.

1. Introduction

The perovskite oxides ABO_3 form a wide family of compounds, reflecting the flexibility in the chemical composition and crystal structure. Structures of perovskite compounds can be regarded as the stacking of close-packed AO_3 layers and the filling of subsequent octahedral sites by B-site ions. The difference in the stacking sequence changes the way of linkage of BO_6 octahedra: the corner-sharing BO_6 in the cubic perovskite (3L: three-layer) with *abc*… sequence, the face-sharing BO_6 in 2L-perovskite (2L: two-layer) with *ab*… sequence, and mixed linkages between the corner- and face-sharing in various intergrowth structures [1].

Since the B cations generally determine the physical properties of perovskite compounds, the combination of different kinds of B cations (B' and B" cations) may bring about attractive properties. When the ratio of the B' and B" cations with different sizes is changed, a variety of the alignment of B' and B" may result, i.e., the stacking sequence of *abc* and *ab* (the corner-and the face-sharing BO_6) is controlled by changing this ratio.

Recently, the 6L-perovskites $Ba_3MM'_2O_9$ (M = alkali metals, alkaline earth elements, 3d transition metals, lanthanides; M' = Ru, Ir) have been investigated [2-22]. In this structure, two $M'O_6$ octahedra are connected by face-sharing and form an M'_2O_9 dimer. These dimers and MO_6 octahedra are placed alternately; thus, 6-layer (6L) structure is generated. The stacking sequence of AO_3 layers is *abacbc*.... For many of these compounds, an antiferromagnetic spin-pairing occurs in the M'_2O_9 dimer even at room temperature. In addition, the $Ba_3MM'_2O_9$ compounds show magnetic transitions at low temperatures, which originates from the magnetic interaction between M and M' ions.

We have been interested in the properties of the perovskites containing pentavalent ruthenium ions. The electronic structure of Ru^{5+} is $[Kr]4d^3$ ([Kr] = krypton electronic core). Such highly oxidized cations from the second transition series sometimes show quite unusual magnetic behavior. Then, we focused our attention on new quadruple perovskites $Ba_4LnRu_3O_{12}$

(Ln = lanthanides) in which the ratio of Ln:Ru is 1:3. In the $Ba_4LnRu_3O_{12}$, three RuO_6 octahedra are face-shared, forming a Ru_3O_{12} trimer, and we thought that peculiar magnetic behavior due to new alignment of the Ln and Ru ions should be observed [23]. In the $Ba_3LnRu_2O_9$, the ground state of the total spin of the isolated Ru_2O_9 dimer may be zero, i.e., $S_{total} = S_1 + S_2 = 0$, for the case that the antiferromagnetic coupling exists between the Ru ions. On the other hand, in the case of $Ba_4LnRu_3O_{12}$ compounds, the total magnetic moment of the Ru_3O_{12} trimer does not disappear as far as three Ru ions are equivalent.

In the preceding paper, we published the results of magnetic susceptibility and specific heat measurements for quadruple perovskites $Ba_4LnRu_3O_{12}$ (Ln = Ce, Pr, Tb) in which the Ln ions are in the tetravalent state [23]. Although no long-range magnetic ordering of Ru^{4+} ions was found for the triple perovskite $Ba_3TbRu_2O_9$, $Ba_4TbRu_3O_{12}$ showed an antiferromagnetic transition at 24 K, which is due to the relatively strong magnetic interaction between Tb^{4+} ions and Ru_3O_{12} trimer via the Tb–O–Ru pathway. In this case, there exists an uncancelled magnetic moment in the Ru_3O_{12} trimer. While no magnetic anomaly was observed down to 0.5 K for $Ba_4CeRu_3O_{12}$, $Ba_4PrRu_3O_{12}$ showed an antiferromagnetic transition at 2.4 K, which should be ascribable to the magnetic Pr^{4+} ions.

In this work, we will report the magnetic properties of quadruple perovskites $Ba_4LnRu_3O_{12}$ (Ln = La, Nd, Sm-Gd, Dy-Lu), and compare their results with those for triple perovskites $Ba_3LnRu_2O_9$.

2. Experimental

2.1. Synthesis

Polycrystalline samples of $Ba_4LnRu_3O_{12}$ (Ln = La–Nd, Sm–Lu) were prepared by the standard solid-state reaction. BaO, BaO_2, Ru, RuO_2, and Ln_2O_3 were used as starting materials. Among them, La_2O_3 and Nd_2O_3 absorb moistures in air and easily form lanthanide hydroxides $Ln(OH)_3$. Therefore, we preheated these compounds at 900 °C for 12 h so as to decompose into

Ln_2O_3 before use. For better reactivity, the thermally decomposed products (500°C for 4 h) of lanthanide nitrates (Ln = Dy, Ho) were used as the lanthanide oxides. These starting materials were weighed out in the appropriate ratio, and well mixed in an agate mortar. The mixtures were pressed into pellets and enclosed with platinum tubes, and then they were sealed in evacuated silica tubes. They were fired at 1250°C for 12–204 h. The obtained phases were identified by powder X-ray diffraction (XRD) measurements. For compounds with Ln = Gd-Lu, impurity phases (for example, 6L-perovskite $Ba_3LnRu_2O_9$ [5, 6, 8, 13-16] or pyrochlore $Ln_2Ru_2O_7$ [24]) were formed due to easy sublimation of Ba oxides and Ru oxides. In order to decrease such an impurity phase, the excess amount of $BaRuO_3$ [25] was added during sample preparation.

2.2. X-ray diffraction analysis

Powder X-ray diffraction profiles were measured using a Rigaku Multi-Flex diffractometer with Cu-Kα radiation equipped with a curved graphite monochromator. The data were collected by step-scanning in the angle range of $10° \leq 2\theta \leq 120°$ at a 2θ step-size of 0.02°. The X-ray diffraction data were analyzed by the Rietveld technique, using the programs RIETAN2000 [26].

2.3. Magnetic susceptibility measurements

The temperature-dependence of the magnetic susceptibility was measured in an applied field of 0.1 T over the temperature range of $1.8\ K \leq T \leq 400\ K$, using a SQUID magnetometer (Quantum Design, MPMS5S). The susceptibility measurements were performed under both zero-field-cooled (ZFC) and field-cooled (FC) conditions. The former was measured upon heating the sample to 400 K under the applied magnetic field of 0.1 T after zero-field cooling to 1.8 K. The latter was measured upon cooling the sample from 400 to 1.8 K at 0.1 T. The field dependence of magnetization for $Ba_4LnRu_3O_{12}$ (Ln = La, Nd, Lu) was measured at 1.8 and 5 K over the applied magnetic field range of $-5\ T \leq H \leq 5T$.

3. Results and Discussion

3.1. Preparation and the structure of $Ba_4LnRu_3O_{12}$

Quadruple perovskite compounds $Ba_4LnRu_3O_{12}$ were prepared for Ln = La–Nd, and Sm–Lu. The results of the powder X-ray diffraction measurements and their Rietveld analysis show that the $Ba_4LnRu_3O_{12}$ for Ln = Tb-Lu have a hexagonal unit cell with space group *R*-3*m* (No.166), while those for Ln = La-Nd, Sm-Gd have a monoclinic unit cell with space group *C*2/*m* (No.12) due to the larger difference in the ionic radius between Ln and Ru [23]. Figures 1 (a) and (b) show the X-ray diffraction profiles for $Ba_4SmRu_3O_{12}$ and $Ba_4ErRu_3O_{12}$, respectively. The refined structural parameters of these two compounds are listed in Tables 1 (a) and (b).

Figure 2 shows the crystal structure of $Ba_4LnRu_3O_{12}$. Three RuO_6 octahedra are connected to each other by face-sharing and form a Ru_3O_{12} trimer. The Ru_3O_{12} trimers and LnO_6 octahedra are alternately linked by corner-sharing. As shown in this figure, the perovskite-type structure with 12 layers is formed (the stacking sequence: *ababcacabcbc*...), which is similar to those for $Ba_4ZrRu_3O_{12}$ [27] and $Ba_4LnMn_3O_{12}$ (Ln = Ce, Pr) [28]. Battle et al. reported that the structures of $Ba_4LiRu_3O_{12}$ and $Ba_4NaRu_3O_{12}$ are 6L and 8L hexagonal perovskite-type structures, respectively [29]. Due to the difference in the charge and size between lanthanides and alkaline metals, $Ba_4LnRu_3O_{12}$ adopts the perovskite-type structure with 12 layers.

The lattice parameters for $Ba_4LnRu_3O_{12}$ are listed in Table 2. Figure 3 shows the variation of lattice parameters with the ionic radius of Ln^{3+} together with those for $Ba_4LnIr_3O_{12}$. Except for the compounds having Ln = Ce, Pr, and Tb, the lattice parameters *a*, *b*, and *c* monotonously increase with the Ln^{3+} ionic radius. However, the values for Ln = Ce, Pr, and Tb compounds are considerably smaller than this trend. These facts strongly indicate that the Ln ions are in the tetravalent state for Ln = Ce, Pr, and Tb compounds. Similar results have been reported in the 6L-perovskites $Ba_3LnM_2O_9$ (M = Ru, Ir) [14, 18]. Therefore, the oxidation states of Ln and Ru are both tetravalent for Ln = Ce, Pr, Tb compounds ($Ba_4Ln^{4+}Ru^{4+}{}_3O_{12}$), and Ln ions are in the trivalent state and the mean oxidation state of Ru ions is +4.33 for other compounds

($Ba_4Ln^{3+}Ru^{4.33+}{}_3O_{12}$).

3.2. Magnetic properties

3.2.1. $Ba_4Ln^{3+}Ru^{4.33+}{}_3O_{12}$ (Ln = La, Lu)

Since La^{3+} and Lu^{3+} ions are diamagnetic, only the Ru ions contribute to the magnetic properties of $Ba_4LnRu_3O_{12}$ (Ln = La, Lu). Figures 4 and 5 show the temperature dependence of the magnetic susceptibility and the reciprocal magnetic susceptibility for $Ba_4LnRu_3O_{12}$ (Ln = La, Lu). Both of these compounds order antiferromagnetically at 6.0 K (Ln = La) and 8.0 K (Ln = Lu). Reciprocal susceptibility vs. temperature curves indicate that the susceptibility does not follow the simple Curie-Weiss law and that the effective magnetic moment decreases with decreasing temperature, especially at lower temperatures. Similar trend has been observed for the triple perovskites $Ba_3LnRu_2O_9$ and $Ba_3LnRuIrO_9$ [15, 20]. On the other hand, corresponding iridium compounds $Ba_4LnIr_3O_{12}$ (Ln = La, Lu) are diamagnetic, indicating that $Ir^{4.33+}{}_3O_{12}$ trimers are diamagnetic [30]. Therefore, we can conclude that the $Ru^{4.33+}{}_3O_{12}$ trimer greatly contributes to the magnetic properties of these compounds.

The distances between Ru atoms in the Ru_3O_{12} trimer are 2.48~2.60 Å, which are shorter than double the metallic radius of Ru (2.68 Å) [31]. The short Ru-Ru interatomic distances in the Ru_3O_{12} trimer suggest the overlap of metal d orbitals having lobes along the threefold symmetry axis, which means the formation of molecular orbitals in the Ru_3O_{12} trimer. The electronic structure of Ru_3Cl_{12} with D_{3d} point symmetry has been described [32]. The energy scheme of Ru_3O_{12} in the $Ba_4LnRu_3O_{12}$ should be similar to the case of Ru_3Cl_{12}. The electronic configuration of the $Ru^{4.33+}{}_3O_{12}$ trimer (the number of 4*d* electrons is 11) with D_{3d} point symmetry is $(a_{1g})^2(e_g)^4(a_{2u})^2(e_u)^3$. The highest occupied e_u orbital has the $S = 1/2$ ground state. Therefore, the $Ru^{4.33+}{}_3O_{12}$ trimer contributes to the magnetic properties of $Ba_4LnRu_3O_{12}$. As mentioned above, the effective magnetic moments decrease with decreasing temperature for these compounds, and they are determined to be 2.86 μ_B above 150 K. Although this value is

larger than the moment expected for S = 1/2, it is much smaller than the moment calculated from the contribution of ($2Ru^{4+} + Ru^{5+}$), 5.57 μ_B (see Table 3). That is, we can accept that the $Ru^{4.33+}{}_3O_{12}$ trimer has the spin S = 1/2.

For both the compounds, $Ba_4LaRu_3O_{12}$ and $Ba_4LuRu_3O_{12}$, the divergence between the ZFC and FC susceptibilities has been observed below the magnetic transition temperature. Since the magnetic hysteresis loop was observed below the transition temperature, these compounds are antiferromagnets with a small ferromagnetic moment (the residual magnetic moment of $Ba_4LaRu_3O_{12}$ is 2×10^{-4} μ_B/mol, and that of $Ba_4LuRu_3O_{12}$ is 1.8×10^{-3} μ_B/mol at 1.8 K).

3.2.2. $Ba_4NdRu_3O_{12}$

Figures 6 (a) and (b) show the temperature dependence of the magnetic susceptibility and the reciprocal susceptibility for $Ba_4NdRu_3O_{12}$. The susceptibility abruptly increases when the temperature is decreased through 11.5 K. Below this temperature, the divergence of the zero-field cooled (ZFC) and field cooled (FC) magnetic susceptibilities was observed. By fitting the Curie-Weiss law to the susceptibility at high temperatures, the effective magnetic moment (μ_{eff}) and the Weiss constant (θ) are obtained to be μ_{eff} = 4.70 μ_B and θ = -140 K. The effective magnetic moments of $Ba_4LnRu_3O_{12}$ are summarized in Table 3. Since both the Ln^{3+} ion and $Ru^{4.33+}{}_3O_{12}$ trimer with S = 1/2 contribute to the magnetic properties of the $Ba_4LnRu_3O_{12}$, its effective magnetic moments should be calculated to be $\mu_{cal} = \sqrt{\mu_{Ln^{3+}}{}^2 + \mu_{S=1/2}{}^2}$, and they are also listed in Table 3. Experimental values are comparable with the calculated moments and are considerably smaller than the moments calculated from the contribution of ($Ln^{3+} + 2Ru^{4+} + Ru^{5+}$). Figure 7 shows the results of the magnetization of $Ba_4NdRu_3O_{12}$ measured at 1.8 and 5 K. Hysteresis loop has been observed in this M-H curve, and the residual magnetization is 0.8 μ_B. The negative Weiss constant indicates that this magnetic behavior is ferrimagnetic rather than ferromagnetic. Neutron diffraction measurements are necessary to determine the magnetic

structure of $Ba_4NdRu_3O_{12}$. One possible magnetic structure is that ferromagnetically aligned Nd ions are antiparallel to the magnetic moments of Ru_3O_{12} trimers. Similar magnetic behavior has been observed for the triple perovskite $Ba_3NdRu_2O_9$, which shows a long-range ferromagnetic ordering of Nd^{3+} ions at 24.0 K [13].

3.2.3. $Ba_4LnRu_3O_{12}$ (Ln = Sm, Eu)

Temperature dependence of the magnetic susceptibilities of $Ba_4SmRu_3O_{12}$ and $Ba_4EuRu_3O_{12}$ is shown in Fig. 8. It is clear that the magnetic susceptibilities do not obey the Curie-Weiss law. For the Sm^{3+} and Eu^{3+} ions, the multiplet levels are not large compared to k_BT (k_B : Boltzmann constant), so the excited state should contribute to the magnetic susceptibility and the temperature dependence of the magnetic susceptibility, in general, becomes complicated. Since the ground state of Eu^{3+} ion is $^7F_0$, i.e., nonmagnetic, there exists some temperature range in which the susceptibility should be independent of temperature, for example, in the temperature range below 50 K. However, the magnetic susceptibility of $Ba_4EuRu_3O_{12}$ still increases with decreasing temperature. This reflects the paramagnetic behavior of $Ru^{4.33+}{}_3O_{12}$ trimers in the $Ba_4EuRu_3O_{12}$.

When the magnetic behavior of $Ru^{4.33+}{}_3O_{12}$ trimers follows the Curie-Weiss law, the molar magnetic susceptibility of $Ba_4SmRu_3O_{12}$ is given by

$$\chi(Ba_4SmRu_3O_{12}) = \chi_{CW} + \chi_{Sm^{3+}} + \chi_{TIP}, \quad (1)$$

where χ_{CW} is the susceptibility of Ru_3O_{12} trimer, and χ_{TIP} is the temperature-independent term containing the diamagnetic term. The ground state of the Sm^{3+} ion is $^6H_{5/2}$. Considering the contribution from the excited states ^6H_J (J =7/2, 9/2, ---, 13/2), the molar magnetic susceptibility of Sm^{3+} can be written by the following equation [33],

$$\chi_{Sm^{3+}} = \frac{N_A \mu_B{}^2 / 3k_B}{\delta T} \frac{2.14\delta + 3.67 + (42.9\delta + 0.82)e^{-7\delta} + (142\delta - 0.33)e^{-16\delta} + \cdots}{3 + 4e^{-7\delta} + 5e^{-16\delta} + \cdots}, \quad (2)$$

where $\delta = \lambda / k_BT$ is the ratio of the over all multiplet width to k_BT. By fitting Eq. (1) to the experimental magnetic susceptibility of $Ba_4SmRu_3O_{12}$, the spin-orbit coupling constant λ of

Sm^{3+}, the effective magnetic moment, μ_{eff}, and the Weiss constant θ were obtained to be λ = 453.2 cm^{-1}, μ_{eff} = 2.88 μ_B, and θ = -349.6 K. The energy difference between the ground state and the first excited state (ΔE_1) is 1586 cm^{-1}, which is near to the values observed for the Sm^{3+} containing compounds. The fitting results of Eq. (1) to the experimental magnetic susceptibility are shown in the Supplemental figure. Similar calculations were performed for the magnetic susceptibility of $Ba_4EuRu_3O_{12}$, and λ = 366 cm^{-1}, μ_{eff} = 1.18 μ_B, and θ = -221.0 K, and ΔE_1 = 366 cm^{-1} were obtained [34]. The effective magnetic moments (μ_{eff}) of $Ba_4SmRu_3O_{12}$ and $Ba_4EuRu_3O_{12}$ are comparable to the moments calculated at room temperature (μ_{cal}*) (Table 3).

The inset of Fig. 8 shows the magnetic susceptibility vs. temperature curves for $Ba_4SmRu_3O_{12}$ and $Ba_4EuRu_3O_{12}$ below 9 K. Both of these compounds indicate an antiferromagnetic ordering at 3.5 K (Ln = Sm) and 4.0 K (Ln = Eu). Since the ground state of Eu^{3+} ion is nonmagnetic, this ion does not contribute to the magnetic ordering. Specific heat measurements for $Ba_4EuRu_3O_{12}$ also show an anomaly at the same temperature, 4.0 K [34]. The analysis of the specific heat data has proved that one unpaired electron of Ru_3O_{12} trimer is responsible for the long-range antiferromagnetic ordering observed at 4.0 K.

3.2.4. $Ba_4LnRu_3O_{12}$ (Ln = Gd, Dy, Ho, Er, Tm, Yb)

Figures 9 (a) and 10 (a) show the temperature dependence of the magnetic susceptibility for $Ba_4GdRu_3O_{12}$ and $Ba_4HoRu_3O_{12}$, respectively. An antiferromagnetic transition is observed at 8.5 K for $Ba_4HoRu_3O_{12}$. For $Ba_4GdRu_3O_{12}$, the first derivative of the magnetic susceptibility against temperature (the inset of Fig. 9) indicates the existence of the magnetic anomaly at 2.5 K. Similar magnetic anomaly has been observed for Ln = Dr, Er, Tm, and Yb compounds at 30, 8.0, 8.5, and 13 K, respectively. For any of these compounds, their Weiss constants are negative, indicating that the magnetic interaction should be antiferromagnetic. The temperature dependences of magnetic susceptibilities and reciprocal susceptibilities for Ln = Dy, Er, Tm, and Yb compounds are summarized in Supplementary figures.

3.2.5. Comparison of magnetic properties of $Ba_4LnRu_3O_{12}$ with those of $Ba_3LnRu_2O_9$ and Ba_2LnRuO_6

Table 4 lists the magnetic transition temperatures for $Ba_{n+1}LnRu_nO_{3n+3}$ (n = 1, 2, 3) in which the Ln ions are in the trivalent state. Magnetic transition temperatures of Ba_2LnRuO_6 are considerably higher than those of the corresponding $Ba_4LnRu_3O_{12}$ and $Ba_3LnRu_2O_9$. This is due to the fact that the magnetic interaction of Ba_2LnRuO_6 is via the almost linear pathway of Ln-O-Ru [36, 37, 40-42]. Therefore, the Ln ions greatly contribute to the antiferromagnetic ordering of Ba_2LnRuO_6, and their transition temperatures are considerably different among Ba_2LnRuO_6 compounds.

The situation for $Ba_4LnRu_3O_{12}$ is quite different from that for Ba_2LnRuO_6. Any of the $Ba_4Ln^{3+}Ru^{4.33+}{}_3O_{12}$ compounds shows magnetic anomaly at lower temperatures. On the other hand, the corresponding iridium compounds $Ba_4Ln^{3+}Ir^{4.33+}{}_3O_{12}$ are paramagnetic down to 1.8 K, and their magnetic properties are due to the magnetic behavior of Ln^{3+} ions [30]. These results indicate that the antiferromagnetic transition observed in the $Ba_4Ln^{3+}Ru^{4.33+}{}_3O_{12}$ is due to the magnetic behavior of the $Ru^{4.33+}{}_3O_{12}$ trimer with S = 1/2. Therefore, its transition temperatures are comparable among $Ba_4LnRu_3O_{12}$ compounds. Similar results have been observed for the antiferromagnetic transition temperatures of $Ba_3Ln^{3+}Ru^{4.5+}{}_2O_9$. The results on magnetic susceptibility and specific heat measurements for $Ba_3LnRu_2O_9$ compounds show that the antiferromagnetic interaction is ascribed to the behavior of $Ru^{4.5+}{}_2O_9$ dimer (S = 1/2) [15, 16].

Acknowledgement

This work was supported by Grant-in-aid from the Ministry of Education, Science, Sports, and Culture of Japan.

References

[1] J. M. Longo and J. A. Kafalas, *J. Solid State Chem.*, **1**, 103−108 (1969).

[2] R. C. Bryne and C. W. Moeller, *J. Solid State Chem.*, **2**, 228−235 (1970).

[3] J. Darriet, M. Drillon, G. Villeneuve, and P. Hagenmuller, *J. Solid State Chem.*, **19**, 213−220 (1976).

[4] H.-U. Schaller and S. Kemmler-Sack, *Z. Anorg. Allg. Chem.*, **473**, 178-188 (1981).

[5] I. Thumm, U. Treiber, and S. Kemmler-Sack, *Z. Anorg. Allg. Chem.*, **477**, 161-166 (1981).

[6] U. Treiber, S. Kemmler-Sack, A. Ehmann, H.-U. Schaller, E. Dürrschmidt, I. Thumm and H. Bader, *Z. Anorg. Allg. Chem.*, **481**, 143-152 (1981).

[7] P. Lightfoot and P. D. Battle, *J. Solid State Chem.*, **89**, 174−183 (1990).

[8] M. Rath and H. Müller-Buschbaum, *J. Alloys Compd.*, **210**, 119-123 (1994).

[9] H. W. Zandbergen and D. J. W. IJdo, *Acta Crystallogr*., C**40**, 919-922 (1984).

[10] D. Verdoes, H. W. Zandbergen, and D. J. W. IJdo, *Acta Crystallogr*., C**41**, 170-173 (1985).

[11] J. T. Rijssenbeek, P. Matl, B. Batlogg, N. P. Ong, and R. J. Cava, *Phys.Rev.*, **58**, 10315−10318 (1998).

[12] J. T. Rijssenbeek, Q. Huang, R. W. Erwin, H. W. Zandbergen, and R. J. Cava, *J. Solid State Chem.*, **146**, 65−72 (1999).

[13] Y. Doi, Y. Hinatsu, Y. Shimojo, and Y. Ishii, *J. Solid State Chem*., **161**, 113-120 (2001).

[14] Y. Doi, M. Wakeshima, Y. Hinatsu, A. Tobo, K. Ohoyama, and Y. Yamaguchi, *J. Mater. Chem*., **11**, 3135–3140 (2001).

[15] Y. Doi, K. Matsuhira, and Y. Hinatsu, *J. Solid State Chem.*, **165**, 317-323 (2002).

[16] Y. Doi and Y. Hinatsu, *J. Mater. Chem.*, **12**, 1792-1795 (2002).

[17] E. Quarez, M. Huve, F. Abraham, and O. Mentre, *Solid State Sciences*, **5**, 951-963 (2003).

[18] Y. Doi and Y. Hinatsu, *J. Phys.: Condens. Matter*., **16**, 2849–2860 (2004).

[19] Y. Doi and Y. Hinatsu, *J. Solid State Chem.*, **177**, 3239-3244 (2004).

[20] M. W. Lufaso and H.-C. zur Loye, *Inorg. Chem.*, **44**, 9143–9153 (2005).

[21] M. W. Lufaso and H.-C. zur Loye, *Inorg. Chem.*, **44**, 9154–9161 (2005).

[22] T. Sakamoto, Y. Doi, and Y. Hinatsu, *J. Solid State Chem.*, **179**, 2595-2601 (2006).

[23] Y. Shimoda, Y. Doi, Y. Hinatsu, and K. Ohoyama, *Chem Mater.*, **20**, 4512-4518 (2008).

[24] N. Taira, M. Wakeshima, and Y. Hinatsu, *J. Phys.: Condens. Matter*., **11**, 6983–6990 (1999).

[25] P.C. Donohue, L. Katz, and R. Ward, *Inorg. Chem.*, **4**, 306–310 (1965).

[26] F. Izumi and T. Ikeda, *Mater. Sci. Forum*, **321–324**, 198–203 (2000).

[27] C. H. De Vreugd, H. W. Zandbergen, and D. J. W. IJdo, *Acta Crystallogr*., C**40**, 1987-1989 (1984).

[28] A. F. Fuentes, K. Boulahya, and U. Amador, *J. Solid State Chem*., **177**, 714-720 (2004).

[29] P. D. Battle, S. H. Kim, and A. V. Powell, *J. Solid State Chem*., **101**, 161-172 (1992).

[30] Y. Shimoda, Y. Doi, M. Wakeshima, and Y. Hinatsu, *J. Solid State Chem*., **182**, 2873-2879 (2009).

[31] A. F. Wells, *Structural inorganic chemistry 5th Ed.*, Oxford Clarendon Press., (1984).

[32] B. E. Bursten, F. A. Cotton, and A. Fang, *Inorg. Chem.*, **22**, 2127-2133 (1983).

[33] J. H. van Vleck, *The Theory of Electric and Magnetic Susceptibilities*, Clarendon, Oxford, 1932.

[34] Y. Shimoda, Y. Doi, M. Wakeshima, and Y. Hinatsu, *Inorg. Chem*., **48**, 9952-9957 (2009).

[35] P. D. Battle, J. B. Goodenough, and R. Price, *J. Solid State Chem*., **46**, 234-244 (1983).

[36] Y. Izumiyama, Y. Doi, M. Wakeshima, Y. Hinatsu, K. Oikawa, Y. Shimojo, and Y. Morii, *J. Mater. Chem.*, **10**, 2364-2367 (2000).

[37] C. Sakai, Y. Doi, Y. Hinatsu, and K. Ohoyama, *J. Phys.: Condens. Matter*., **17**, 7383–7394 (2005).

[38] T. C. Gibb and R. Greatrex, *J. Solid State Chem*., **34**, 279-288 (1980).

[39] Y. Hinatsu and Y. Doi, *Bull. Chem. Soc. Japan*, **76**, 1093-1113 (2004).

[40] Y. Hinatsu, Y. Izumiyama, Y. Doi, A. Alemi, M. Wakeshima, A. Nakamura, and Y. Morii, *J. Solid State Chem*., **177**, 38-44 (2004).

[41] Y. Izumiyama, Y. Doi, M. Wakeshima, Y. Hinatsu, A.Nakamura, and Y. Ishii, *J. Solid State Chem*., **169**, 125-130 (2002).

[42] Y. Doi, Y. Hinatsu, A. Nakamura, Y. Ishii, and Y. Morii, *J. Mater. Chem.*, **13**, 1758-1763 (2003).

[43] P. D. Battle and C. W. Jones, *J. Solid State Chem*., **78**, 108-116 (1989).

Figure captions

Fig. 1 X-ray diffraction profiles of (a) $Ba_4SmRu_3O_{12}$ and (b) $Ba_4ErRu_3O_{12}$. The calculated and observed profiles are shown on the top solid line and cross markers, respectively. The vertical marks in the middle show positions calculated for Bragg reflections. The lower trace is a plot of the difference between calculated and observed intensities. The insets show the profiles between $26^\circ \leq 2\theta \leq 32^\circ$.

Fig. 2 Schematic crystal structures of $Ba_4LnRu_3O_{12}$. (a): monoclinic unit cell for Ln = La – Nd, Sm – Gd compounds (space group: *C*2/m), (b): hexagonal unit cell for Ln = Tb – Lu compounds (space group: *R*-3m).

Fig. 3 The variation of lattice parameters for $Ba_4LnRu_3O_{12}$ against the ionic radius of Ln^{3+}.The lattice parameters of $Ba_4LnIr_3O_{12}$ are also plotted in this figure.

Fig. 4 (a) Temperature dependence of the magnetic susceptibilities for $Ba_4LaRu_3O_{12}$. The inset shows the magnetic susceptibilities at low temperatures.

(b) The reciprocal magnetic susceptibility against temperature.

Fig. 5 (a) Temperature dependence of the magnetic susceptibilities for $Ba_4LuRu_3O_{12}$. The inset shows the magnetic susceptibilities at low temperatures.

(b) The reciprocal magnetic susceptibility against temperature.

Fig. 6 (a) Temperature dependence of the magnetic susceptibilities for $Ba_4NdRu_3O_{12}$. The inset shows the magnetic susceptibilities at low temperatures.

(b) The reciprocal magnetic susceptibility against temperature.

Fig. 7 Magnetic hysteresis curves for $Ba_4NdRu_3O_{12}$ measured at (a) 1.8 K and (b) 5 K.

Fig. 8 Temperature dependence of the magnetic susceptibilities for $Ba_4SmRu_3O_{12}$ and $Ba_4EuRu_3O_{12}$. The inset shows the magnetic susceptibilities at low temperatures.

Fig. 9 (a) Temperature dependence of the magnetic susceptibilities for $Ba_4GdRu_3O_{12}$. The insets show the magnetic susceptibilities at low temperatures and the first derivative of

the susceptibility against temperature. (b) The reciprocal magnetic susceptibility against temperature. The solid line is the Curie-Weiss fitting.

Fig.10. (a) Temperature dependence of the magnetic susceptibilities for $Ba_4HoRu_3O_{12}$. The inset shows the magnetic susceptibilities at low temperatures. (b) The reciprocal magnetic susceptibility against temperature. The solid line is the Curie-Weiss fitting.

Table 1 (a) Structural parameters for $Ba_4SmRu_3O_{12}$; Space group *C*2/*m* (No.12), *z* = 6.

Atom	Site	*x*	*y*	*z*	*B* / Å^{2} *
a = 10.207(5) Å, *b* = 5.8989(3) Å, *c* = 29.338(2) Å, *β* = 91.38(1) °					
R_{wp} = 12.99 %, R_I = 2.38 %, R_e = 6.36 %					
Ba(1)	4*i*	0.330(3)	0	0.537(1)	0.60(4)
Ba(2)	4*i*	0.339(3)	0	0.385(1)	0.60
Ba(3)	4*i*	-0.010(3)	0	0.286(1)	0.60
Ba(4)	4*i*	0.331(3)	0	0.798(1)	0.60
Ba(5)	4*i*	0.003(3)	0	0.129(1)	0.60
Ba(6)	4*i*	0.333(3)	0	0.951(1)	0.60
Sm(1)	4*i*	0.328(3)	0	0.668(2)	0.47(6)
Sm(2)	2*a*	0	0	0	0.47
Ru(1)	2*c*	0	0	1/2	0.72(5)
Ru(2)	4*i*	0.006(4)	0	0.414(1)	0.72
Ru(3)	4*i*	0.324(4)	0	0.253(1)	0.72
Ru(4)	4*i*	0.334(4)	0	0.167(1)	0.72
Ru(5)	4*i*	0.341(4)	0	0.081(1)	0.72
O(1)	4*i*	0.157(5)	0	0.459(2)	1.0(1)
O(2)	4*i*	0.121(6)	0	0.638(2)	1.0
O(3)	4*i*	0.511(5)	0	0.276(2)	1.0
O(4)	4*i*	0.823(5)	0	0.790(2)	1.0
O(5)	4*i*	0.496(5)	0	0.128(2)	1.0
O(6)	4*i*	0.808(6)	0	0.959(2)	1.0
O(7)	8*j*	0.424(5)	0.739(6)	0.457(2)	1.0
O(8)	8*j*	0.416(4)	0.744(6)	0.617(2)	1.0
O(9)	8*j*	0.222(5)	0.746(5)	0.710(2)	1.0
O(10)	8*j*	0.095(4)	0.742(5)	0.791(2)	1.0
O(11)	8*j*	0.246(4)	0.716(5)	0.880(2)	1.0
O(12)	8*j*	0.048(6)	0.705(6)	0.950(2)	1.0

*The temperature factors (*B*) were fixed on the same values for each element.

Table 1 (b) Structural parameters for $Ba_4ErRu_3O_{12}$; Space group *R*-3*m* (No.166), z = 3.

Atom	Site	*x*	*y*	*z*	*B* / Å^2
a = 5.8559(6) Å, *c* = 29.014(3) Å					
R_{wp} = 9.39 %, R_I = 1.78 %, R_e = 5.61 %					
Ba(1)	6*c*	0	0	0.1290(1)	0.70(5)
Ba(2)	6*c*	0	0	0.2858(1)	0.70
Er	3*a*	0	0	0	0.25(6)
Ru(1)	3*b*	0	0	1/2	0.60(7)
Ru(2)	6*c*	0	0	0.4127(1)	0.60
O(1)	18*h*	0.4899(6)	0.5101	0.1235(3)	1.1(1)
O(2)	18*h*	0.4903(7)	0.5097	0.2901(3)	1.1

*The temperature factors (*B*) were fixed on the same values for each element.

Table 2 Lattice parameters for $Ba_4LnRu_3O_{12}$ (Ln = La-Lu).

Ln	space group	*a* / Å	*b*/ Å	*c* / Å	*β* / °	R_{WP} / %	R_I / %	*S*
La		10.263(6)	5.9363(2)	29.852(3)	92.080(8)	11.91	3.20	1.31
Ce		10.170(3)	5.8767(6)	29.374(5)	90.871(0)	14.57	3.88	1.24
Pr		10.156(6)	5.8694(4)	29.315(2)	90.909(4)	14.03	6.79	1.54
Nd	*C*2/*m*	10.232(2)	5.9142(8)	29.464(7)	91.712(5)	13.89	2.96	1.24
Sm		10.207(5)	5.8989(3)	29.338(2)	91.378(7)	12.99	2.38	1.24
Eu		10.202(6)	5.8950(5)	29.249(8)	91.022(7)	14.41	3.19	1.28
Gd		10.191(2)	5.8873(2)	29.197(9)	90.634(2)	11.03	1.98	1.36
Tb		5.8306(0)	—	29.013(2)	90	11.28	5.62	1.37
Dy		5.8649(1)	—	29.066(6)	90	11.69	2.50	1.50
Ho		5.8625(9)	—	29.032(7)	90	11.00	2.87	1.38
Er	*R*-3*m*	5.8559(6)	—	29.014(3)	90	9.39	1.78	1.67
Tm		5.8478(1)	—	28.962(6)	90	9.27	3.75	1.71
Yb		5.8410(9)	—	28.937(9)	90	13.69	3.37	2.71
Lu		5.8328(1)	—	28.891(2)	90	11.34	2.10	1.50

Definition of reliability factors R_{wp}, R_I and *S* are given as follows:

$R_{\mathrm{WP}} = \left[\sum w\left(\left|F(o)\right| - \left|F(c)\right|\right)^2 / \sum w\left|F(\mathrm{o})\right|^2\right]^{\frac{1}{2}}$, $R_{\mathrm{I}} = \sum \left|I_k(o) - I_k(c)\right| / \sum I_k(o)$, and

$S = \left[\frac{\sum_i w_i \left\{F(o)_i - F(c)_i\right\}^2}{N - P}\right]$.

Table 3 Effective magnetic moments of $Ba_4LnRu_3O_{12}$ (Ln = La-Lu).

Ln	electronic configuration	J	μ_{eff}/μ_B	μ_{cal}^{*}/μ_B	μ_{cal}^{**}/μ_B
La^{3+}	$4f^0$	0	2.86	1.73	5.57
Nd^{3+}	$4f^3$	9/2	4.70	4.01	6.64
Sm^{3+}	$4f^5$	5/2	2.88	2.29 ***	5.63
Eu^{3+}	$4f^6$	0	1.18	1.73 ***	5.57
Gd^{3+}	$4f^7$	7/2	8.24	8.13	9.70
Dy^{3+}	$4f^9$	15/2	11.20	10.77	12.00
Ho^{3+}	$4f^{10}$	8	10.79	10.74	11.97
Er^{3+}	$4f^{11}$	15/2	9.72	9.74	11.09
Tm^{3+}	$4f^{12}$	6	7.75	7.77	9.40
Yb^{3+}	$4f^{13}$	7/2	4.70	4.86	7.18
Lu^{3+}	$4f^{14}$	0	2.86	1.73	5.57

Note: * $\mu_{cal} = \sqrt{\mu_{Ln^{3+}}^{\ 2} + \mu_{S=1/2}^{\ 2}}$.

** $\mu_{cal} = \sqrt{\mu_{Ln^{3+}}^{\ 2} + 2\mu_{Ru\,4+}^{\ 2} + \mu_{Ru\,5+}^{\ 2}}$.

*** These values are calculated using the moments of Ln^{3+} ions at room temperature.

Table 4 Magnetic transition temperatures for $Ba_{n+1}LnRu_nO_{3n+3}$ (n = 1, 2, 3).

Ln^{3+}	Ba_2LnRuO_6 (n = 1)	[Ref.]	$Ba_3LnRu_2O_9$ (n = 2)	[Ref.]	$Ba_4LnRu_3O_{12}$ (n = 3)
La^{3+}	29.5 K	[35]	6.0 K	[15]	6.0 K
Nd^{3+}	57 K	[36]	24.0 K	[13]	11.5 K
Sm^{3+}	54 K	[37]	12.5 K	[15]	3.5 K
Eu^{3+}	42 K	[38]	9.5 K	[15]	4.0 K
Gd^{3+}	48 K	[37]	14.8 K	[16]	2.5 K
Dy^{3+}	47 K	[37]	27.8 K	[39]	30 K
Ho^{3+}	51 K	[40]	10.2 K	[16]	8.5 K
Er^{3+}	40 K	[41]	6.0 K	[16]	8.0 K
Tm^{3+}	42 K	[42]	8.3 K	[16]	8.5 K
Yb^{3+}	48 K	[42]	4.5 K	[16]	13 K
Lu^{3+}	35 K	[43]	9.5 K	[15]	8.0 K

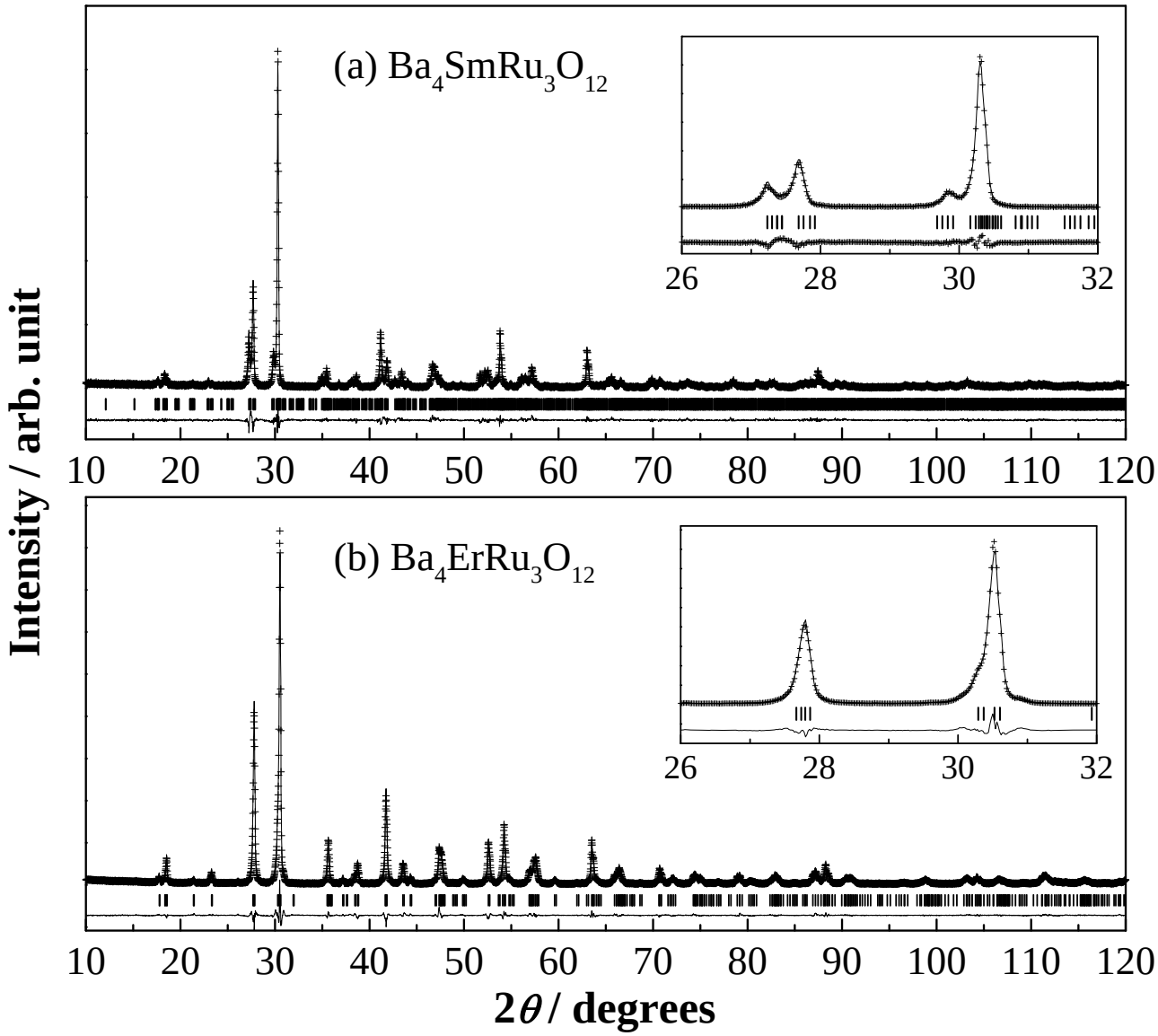
(a) Ba4SmRu3O12
(b) Ba4ErRu3O12
Intensity / arb. unit
2θ / degrees
10 20 30 40 50 60 70 80 90 100 110 120
26 28 30 32

Fig. 1

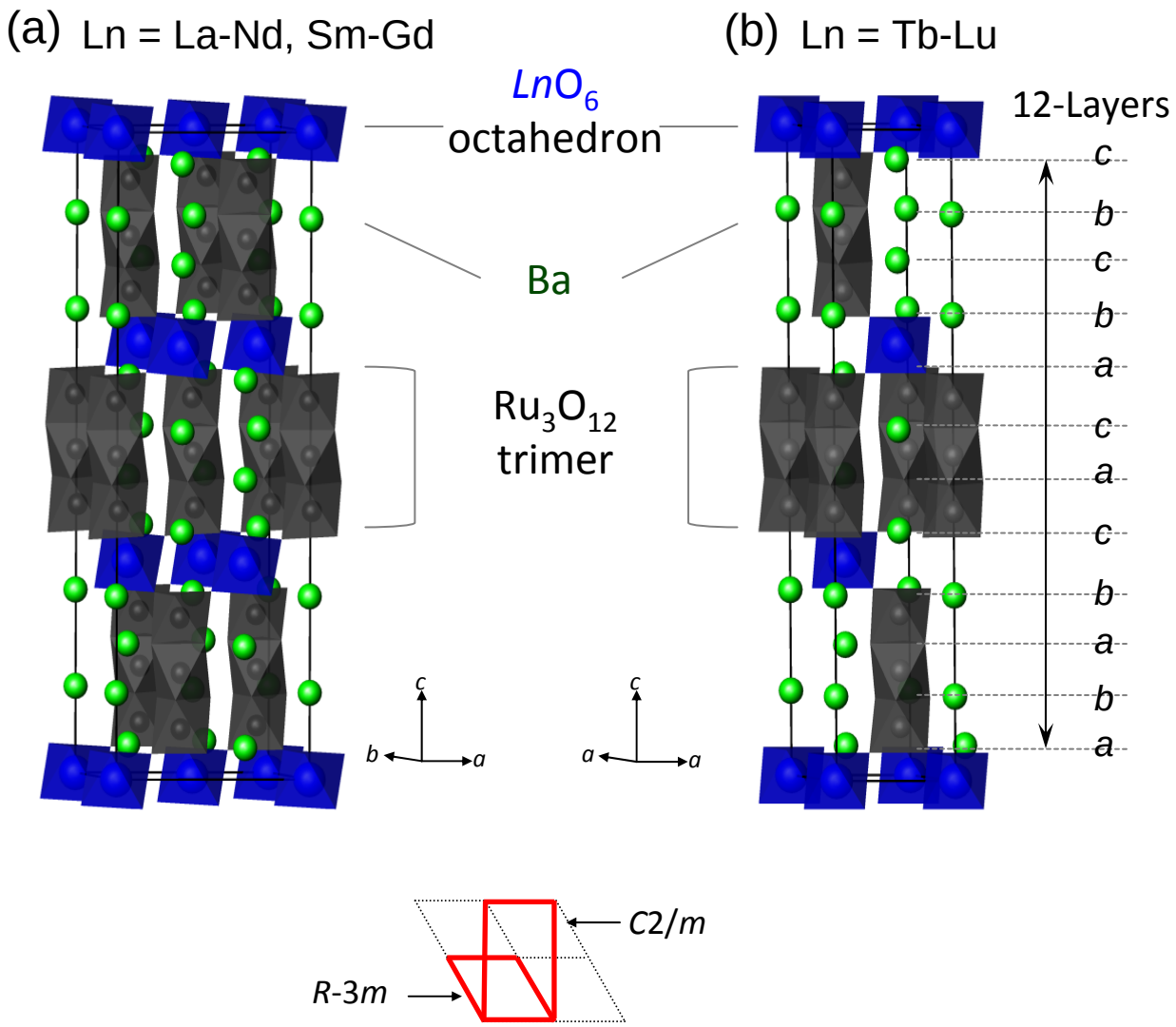
(a) Ln = La-Nd, Sm-Gd
(b) Ln = Tb-Lu
LnO6
octahedron
Ba
Ru3O12
trimer
12-Layers
c
b
c
b
a
c
a
c
b
a
b
a
c
b
a
c
a
a
C2/m
R-3m

Fig. 2

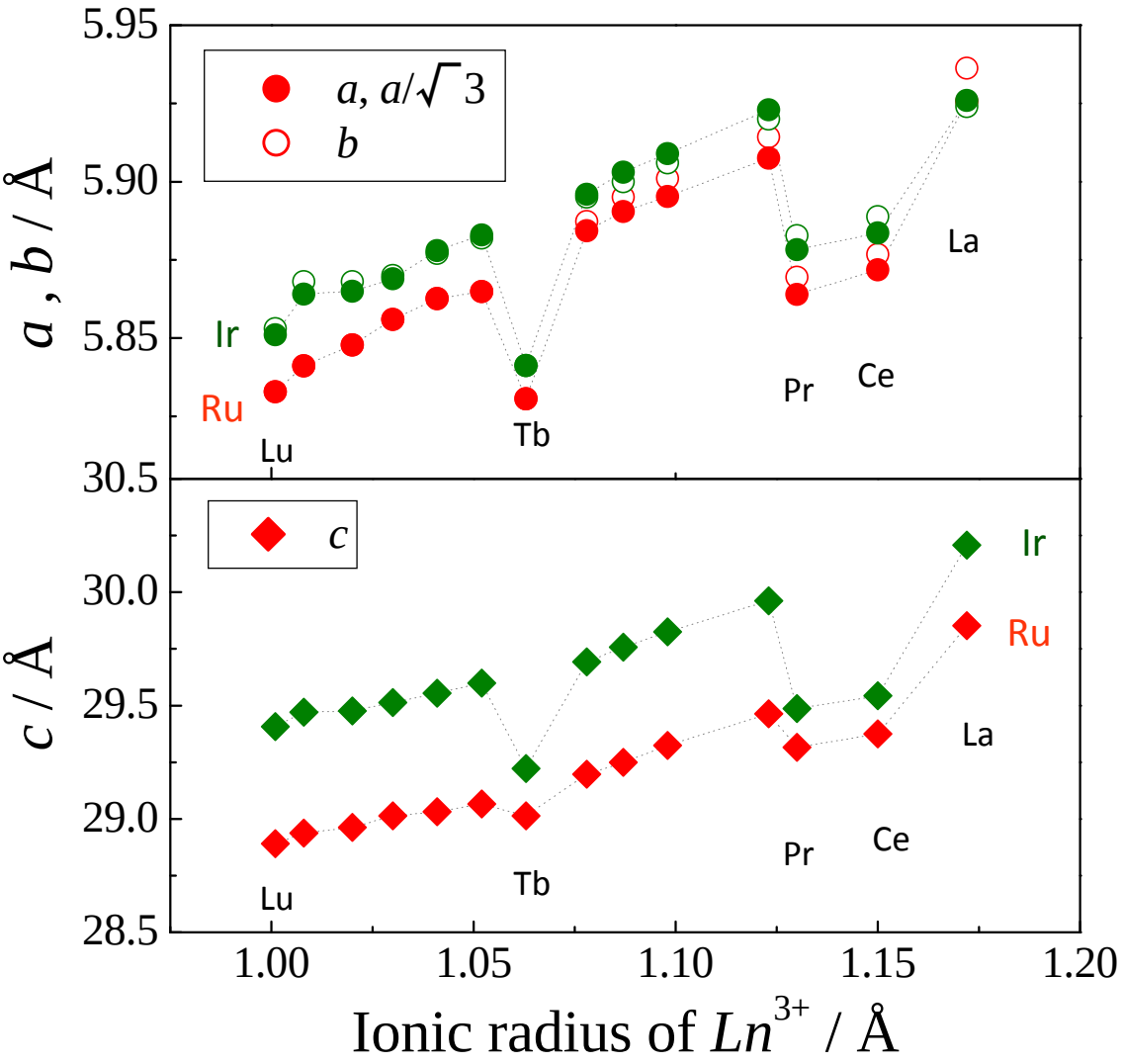
a, a/√3
b
c
Ir
Ru
Lu
Tb
Pr
Ce
La
a , b / Å
c / Å
Ionic radius of Ln3+ / Å
5.95
5.90
5.85
30.5
30.0
29.5
29.0
28.5
1.00
1.05
1.10
1.15
1.20

Fig. 3

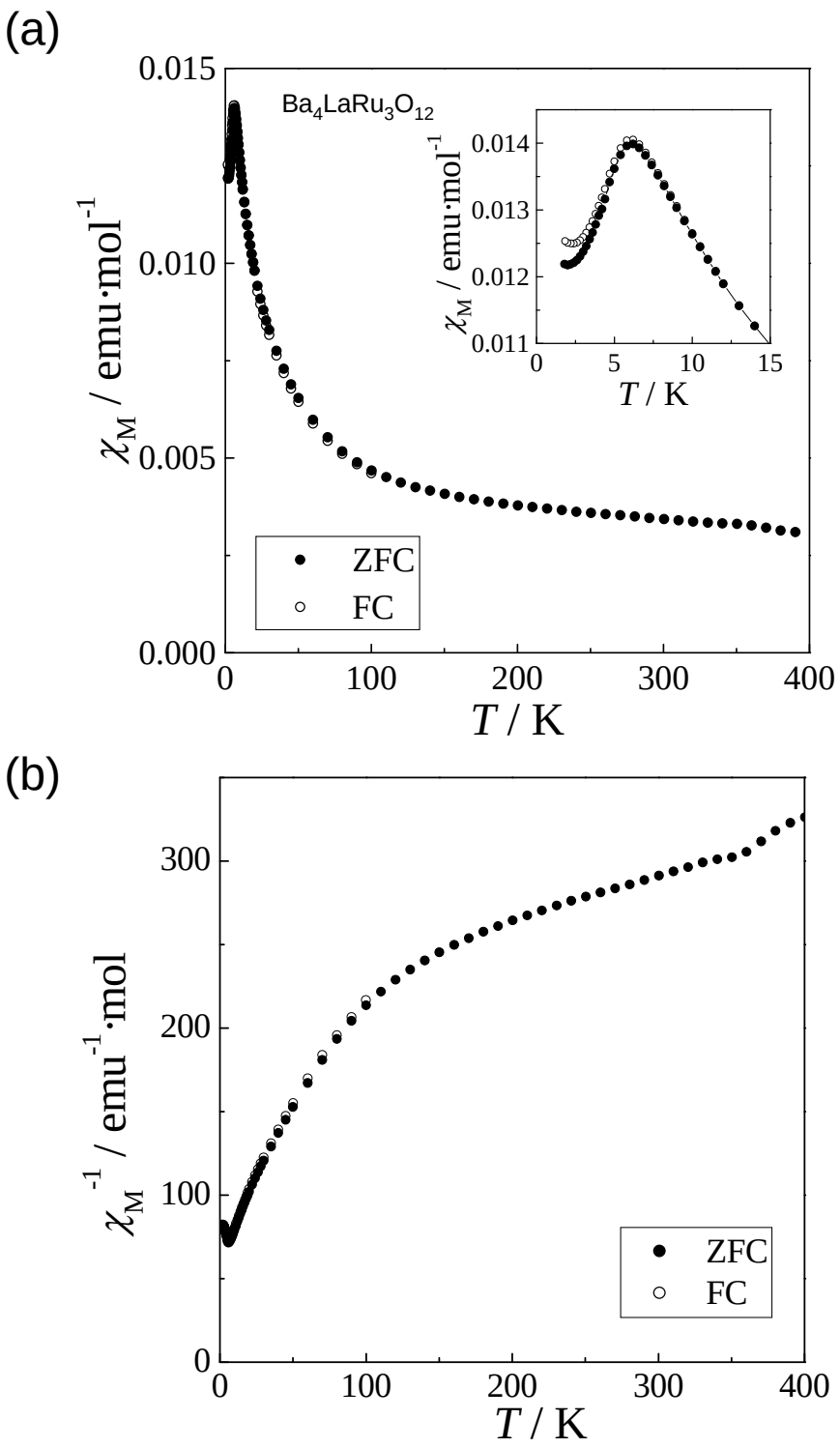
(a)
Ba4LaRu3O12
χM / emu·mol-1
T / K
ZFC
FC
0.015
0.010
0.005
0.000
0
100
200
300
400
0.014
0.013
0.012
0.011
5
10
15
(b)
χM-1 / emu-1·mol
300
200
100
0

Fig. 4

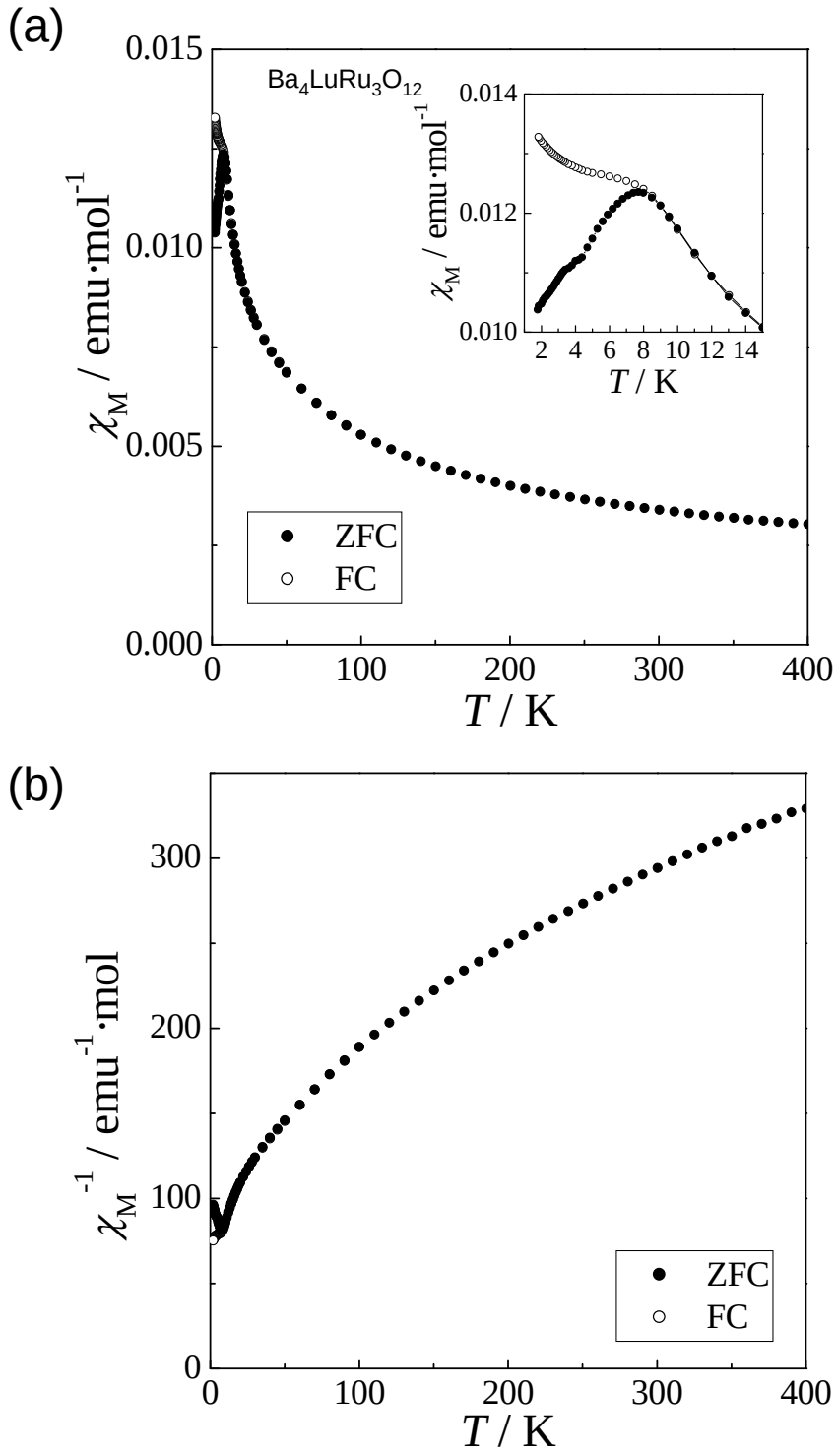
(a)
Ba4LuRu3O12
χM / emu·mol-1
T / K
ZFC
FC
0.015
0.010
0.005
0.000
0
100
200
300
400
0.014
0.012
0.010
2
4
6
8
10
12
14
(b)
χM-1 / emu-1·mol
300
200
100
0

Fig. 5

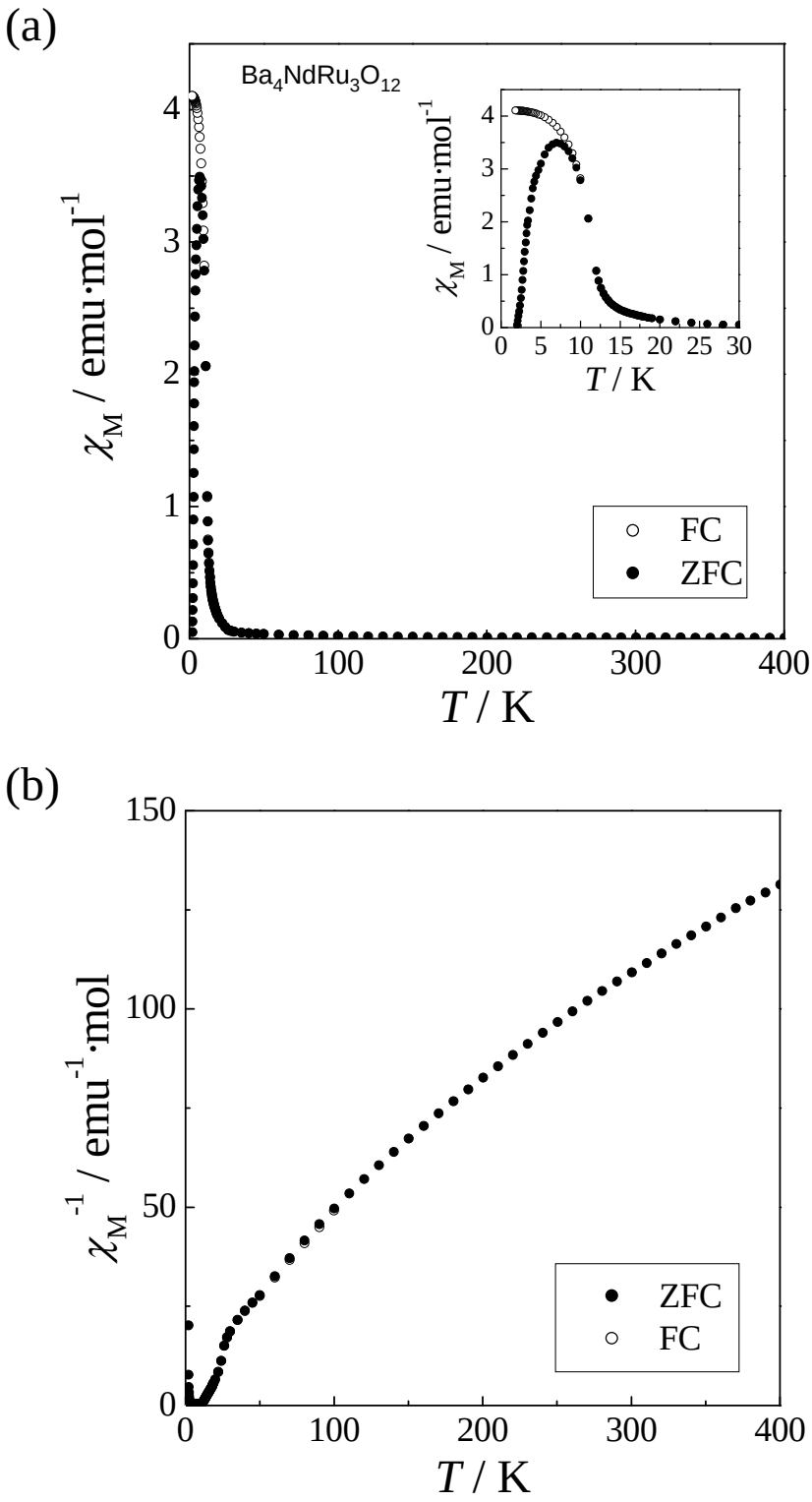

Fig. 6

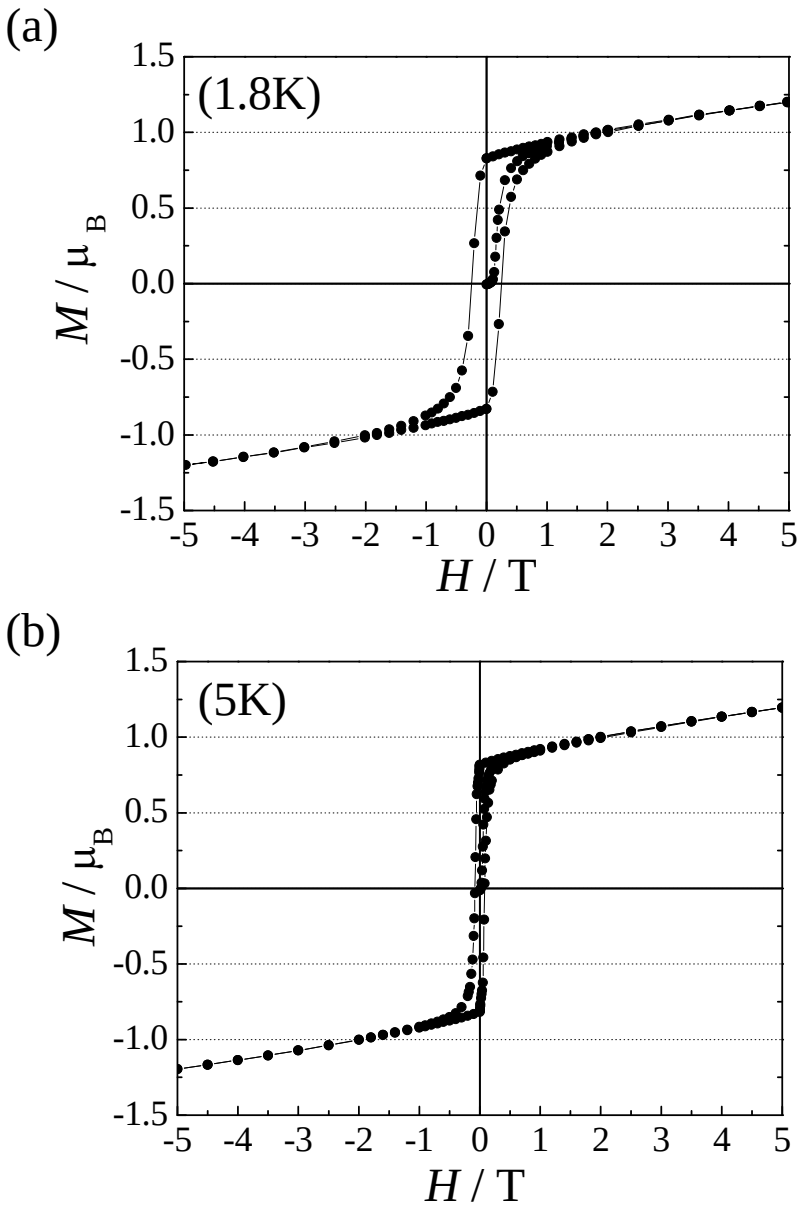

Fig. 7

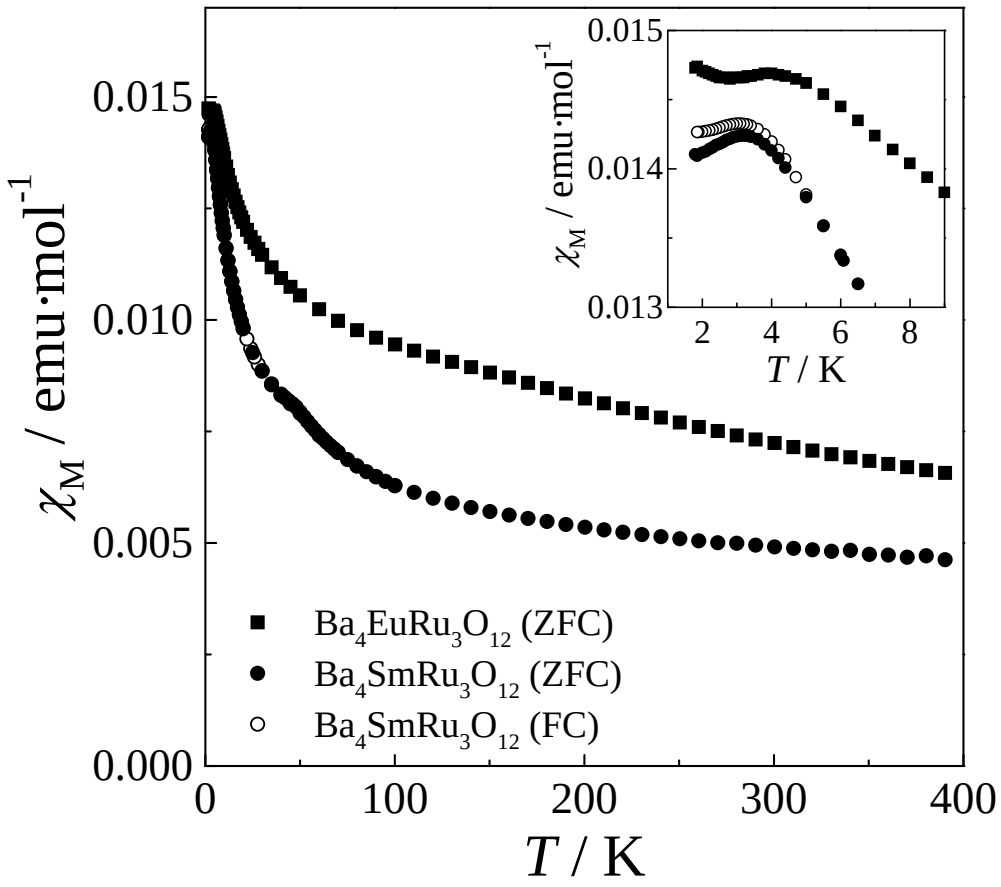
0.015
0.010
0.005
0.000
χM / emu·mol-1
0
100
200
300
400
T / K
Ba4EuRu3O12 (ZFC)
Ba4SmRu3O12 (ZFC)
Ba4SmRu3O12 (FC)
0.015
0.014
0.013
χM / emu·mol-1
2
4
6
8
T / K

Fig. 8

(a)

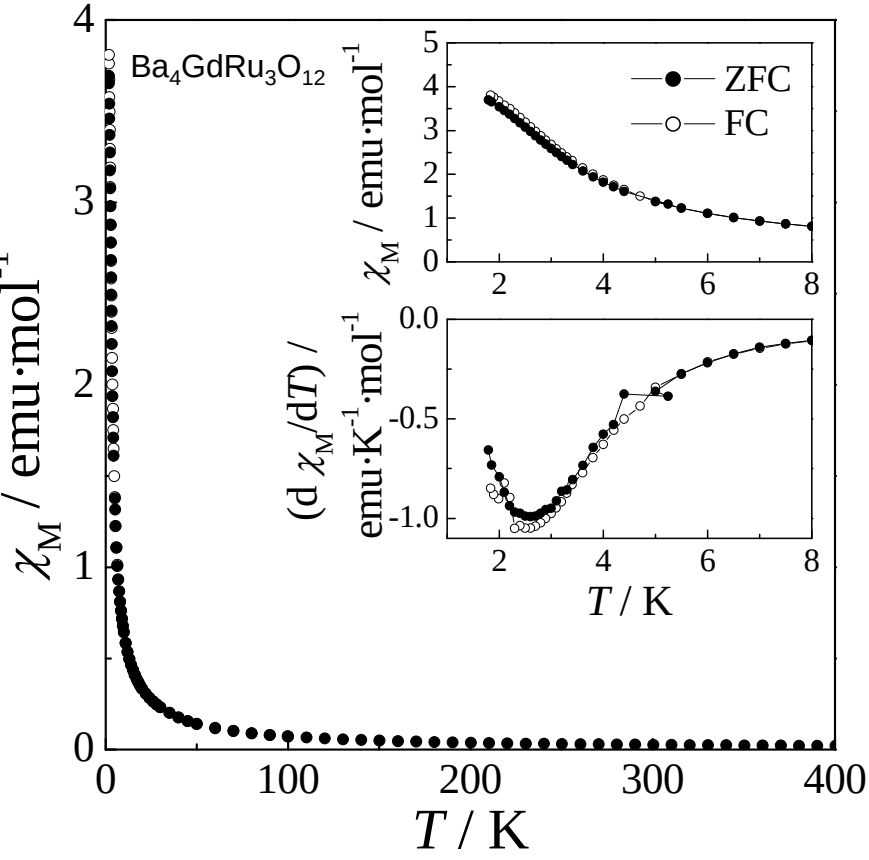
Ba4GdRu3O12
χM / emu·mol-1
T / K
ZFC
FC
χM / emu·mol-1
(d χM/dT) / emu·K-1·mol-1
T / K

(b)

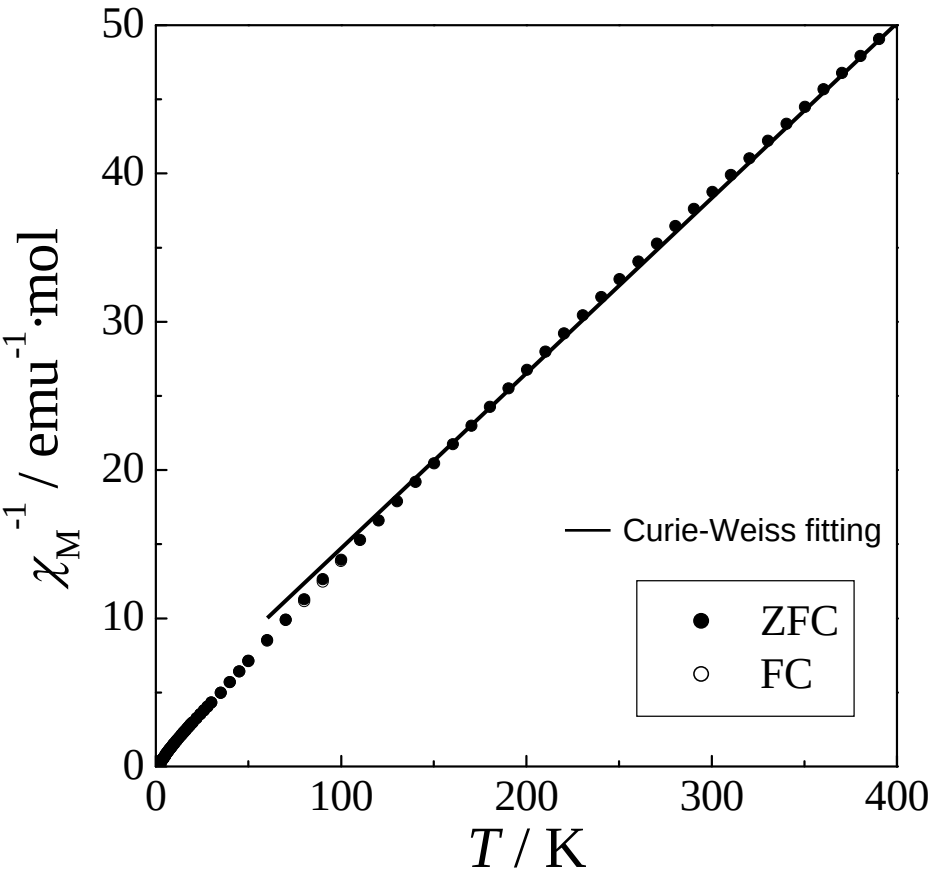
χM-1 / emu-1·mol
T / K
Curie-Weiss fitting
ZFC
FC

Fig. 9

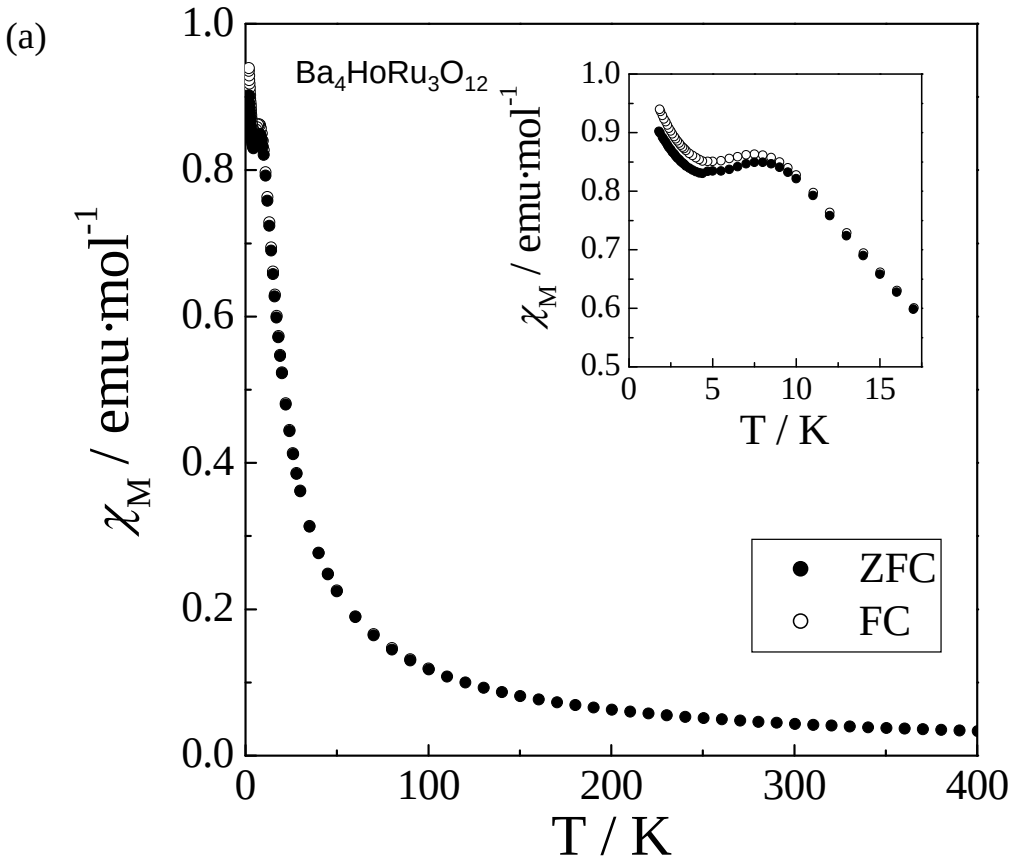
(a)
$Ba_4HoRu_3O_{12}$
χ_M / emu·mol^{-1}
T / K
ZFC
FC
1.0
0.8
0.6
0.4
0.2
0.0
0
100
200
300
400
0.9
0.7
0.5
5
10
15

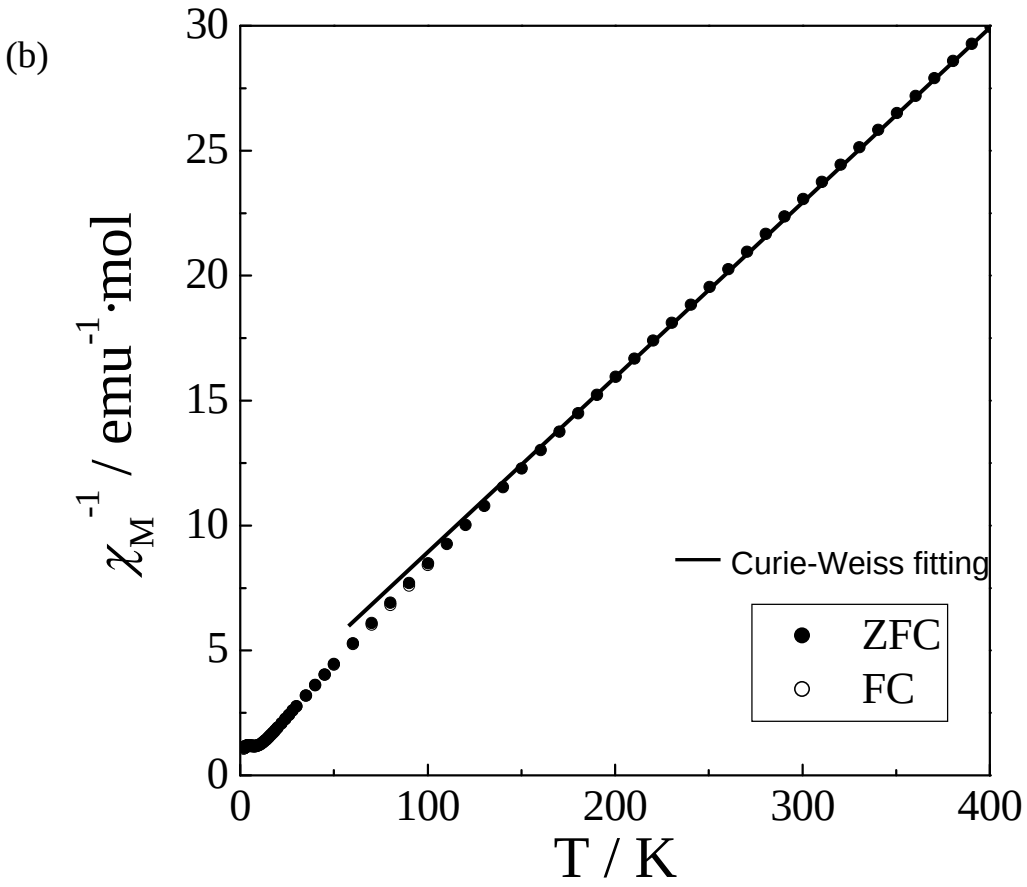
(b)
χ_M^{-1} / emu^{-1}·mol
T / K
Curie-Weiss fitting
ZFC
FC
30
25
20
15
10
5
0
0
100
200
300
400

Fig. 10